Reduced Embedded Magnetic Field in Type-II Superconductor of Finite Dimension

Frances Zhu[1]
Assistant Researcher
Hawai'i Institute of Geophysics and Planetology
University of Hawai'i at Manoa
Honolulu, HI, 96822

Mason A. Peck
Associate Professor
Sibley School of Mechanical and Aerospace Engineering
Cornell University
Ithaca, NY, 14850

Laura L. Jones-Wilson
Guidance and Control Systems Engineer
Jet Propulsion Laboratory
Pasadena, CA, 91803

This work maps the magnetic field within a type-II superconductor of finite dimension that is magnetically flux-pinned. The measured field is lower in magnitude than anticipated from the frozen image model and changes shape dependent on the field-cooled image location. A proposed refined model more accurately reflects the measured field.

I. Introduction

When a type–II superconductor is cooled below its flux-pinning critical temperature in the presence of the magnetic field, the shielding currents within the superconductor persist even after the magnetic field source has been removed. This unique behavior may be exploited to generate passive forces and torques in six degrees-of-freedom that minimize the difference between the magnetic field of an external magnetic moment object and the field in which the superconductor was initially cooled.

The critical state model and the advanced frozen image model are two conventional methods of modeling magnetization behavior for a system of magnets and type–II superconductors. Both models macroscopically represent changes in the superconductor's embedded magnetic field as external field changes but differ in magnetization expression, complexity, and scope of modeling a superconducting system. Valid for an arbitrary superconductor geometry and magnetic field gradient, the critical-state model is very precise but requires immense computation [1] [2]. Kordyuk's frozen image model geometrically maps a magnetic field source as a dipole into paramagnetic and diamagnetic image reflected across the superconductor boundary and moving virtually within the superconductor volume for each independent magnet and superconductor interaction [3]. The frozen image model is analytically compact and is accurate if the model assumptions match the physical system. The critical state model compounds across every mesh node P of each object, requiring an order of $\mathcal{O}(P_M^2 P_N^4)$, more computation than Kordyuk's model, where M and N are numbers of superconductors and magnets respectively. The simplicity of the frozen image model enables the dynamic simulation of real-time applications and systems of many magnets and superconductors, which can have natural modes as fast as hundreds of Hertz. The trade-off in simplicity permeates into assumptions about the superconducting system, which reduces the model's fidelity.

II. Frozen Image Model for Ideal Type-II Superconductors

Kordyuk's frozen image model provides an exact analytical solution for the case of a magnetic dipole's field imprinted to a flat, hard, infinite plane superconductor in the field-cooling process [3]. The total magnetic field generated by the superconductor using the frozen image model is the sum of contributions from the

[1] Corresponding author. email: zhu@higp.hawaii.edu ; phone number: (913) 777-9595

frozen and the mobile images' strength, location, and orientation, given in Eq. (1) and shown in Fig. 1. For an explicit derivation and definition of the flux-pinned dynamics model as well as a comprehensive list of physical parameters that affect the subsequent dynamics, refer to [4] and [5]. The analytical expressions for force and torque are essential for the equations of motion. The potential energy characterizes stability and offers intuition into the macroscopic dynamic behavior of the system. Ultimately, the magnetic field provides the fundamental basis for the physics, which then defines the dynamic behavior of the system.

$$\boldsymbol{B}(\boldsymbol{r}) = \boldsymbol{B_f}(\boldsymbol{r} - \boldsymbol{r_f}, \boldsymbol{m_f}) + \boldsymbol{B_m}(\boldsymbol{r} - \boldsymbol{r_m}, \boldsymbol{m_m}) \quad (1)$$

$$\boldsymbol{r_f} = \boldsymbol{r_{FC}} - 2\big((\boldsymbol{r_{FC}} - \boldsymbol{O_s}) \cdot \boldsymbol{a_s}\big)\boldsymbol{a_s} \quad (2)$$

$$\boldsymbol{r_m} = \boldsymbol{r_{mag}} - 2\Big(\big(\boldsymbol{r_{mag}} - \boldsymbol{O_s}\big) \cdot \boldsymbol{a_s}\Big)\boldsymbol{a_s} \quad (3)$$

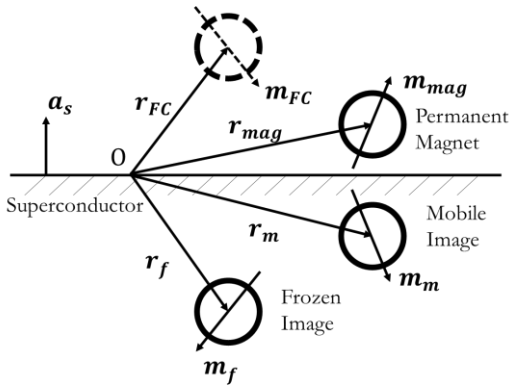

Fig. 1: The permanent magnetic dipole is shown above the superconductor surface. The frozen image dipole is in its field-cooled position. The mobile dipole image mirrors any movement of the permanent magnet after field cooling.

Kordyuk's model does not explicitly define the reference point, $\boldsymbol{O_s}$, on the superconductor surface because a point on an infinite plane may be arbitrarily defined, seen in Eq. (2) and (3). For a real superconductor of finite dimension, the amount of magnetic flux from the magnetic field source that penetrates the superconductor volume varies with distance from the superconductor surface. Previous works show that geometry or spatial relationship of either the magnet or the superconductor affects the strength of the image interaction: shape of the magnet [6], thickness of the superconductor [7], ratio of magnet to superconductor size [8], and source magnet's field shape [9]. To compensate for the finite dimension effect, a distance is measured with respect to the reference point, which should be defined to yield a direct, straightforward relationship between distance and magnetic flux. With the advantage of symmetry, the simplest definition for the reference point is the center of the finite superconductor surface.

III. Finite Plane Effect on Type-II Superconductors

The frozen image model, as applied to an ideal type-II superconductor and a perfect magnetic dipole system, models only these ideal superconductors. This paper explores the change in the system dynamics of the flux-pinned interface for the practical case of finite-dimensioned superconductors. The finite dimension effect is investigated by correlating experimentally measured magnetic fields of the superconductor with the Kordyuk's frozen image model. The present study assesses the finite dimension effect by characterizing a single-domain 56 mm diameter, 16 mm thick YBCO sample in the presence of a 0.75 inch diameter spherical, N42 Neodymium magnet with a surface field of 8815 Gauss. For uniformly magnetized spheres, the magnetic dipole representation is exact everywhere outside of the

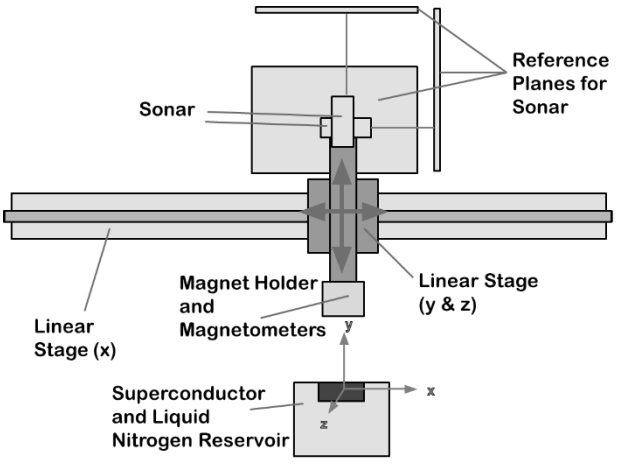

Fig. 2: Top view of linear stage experiment testbed to spatially map magnetic flux of magnets and images within superconductors.

physical magnet sphere [10]. This study's approach to quantifying the finite dimension effect centers on empirical data of the flux-pinned magnetic fields generated by the shielding currents within the superconductor. The experiments were designed to isolate the finite dimension effect on magnetic field flux pinning by varying only field-cooled positions.

A testbed, shown in Fig. 2, measures these resultant magnetic fields. The entire testbed consists of a three degree-of-freedom linear stage, three position sensors, three Hall sensors, one spherical permanent magnet, one cylindrical YBCO superconductor, and a liquid-nitrogen reservoir. The linear stage translates a permanent magnet and sensor package in three degrees-of-freedom. Three SICK ultrasonic sensors, with 0.0168 mm resolution and 3 – 35 cm range, measure the position of the Hall sensors and of the permanent magnet. All magnetic measurements are sampled at 0.1 mm in x position, and 5 mm in y and z position. Three programmable analog Hall sensors from Sensor Solutions M12-PAH-5VSB5, with a range from -1000 Gauss to 1000 Gauss, are aligned such that they are mutually perpendicular to measure the magnetic field in the three spatially orthogonal directions. The spherical magnet provides a magnetic field source during field cooling and a mobile-image dipole source during experiment. The liquid-nitrogen tank serves as a heat sink that maintains the temperature of the YBCO below a critical temperature of 88 K. Two sets of experiments were conducted to investigate finite dimension effects: the first set aimed to look only at the frozen image and the second to look at both the frozen image and the mobile image together. Across all experiments, the magnetic moment points normal to the superconductor surface and verified to align within 2.5 degrees. To isolate the frozen image, the magnet is static while field-cooling the superconductor, and afterwards, the magnet is taken away to be replaced with the three magnetometers. To measure both the frozen and mobile image, the superconductor is field-cooled as before, then, the magnetometer is installed with the magnet on top of the magnetometer. After mapping the magnetic field, the measured magnetic field extrema locations are compared to extrema locations generated by the frozen image model magnetic field, separated into three orthogonal (x, y, and z) components.

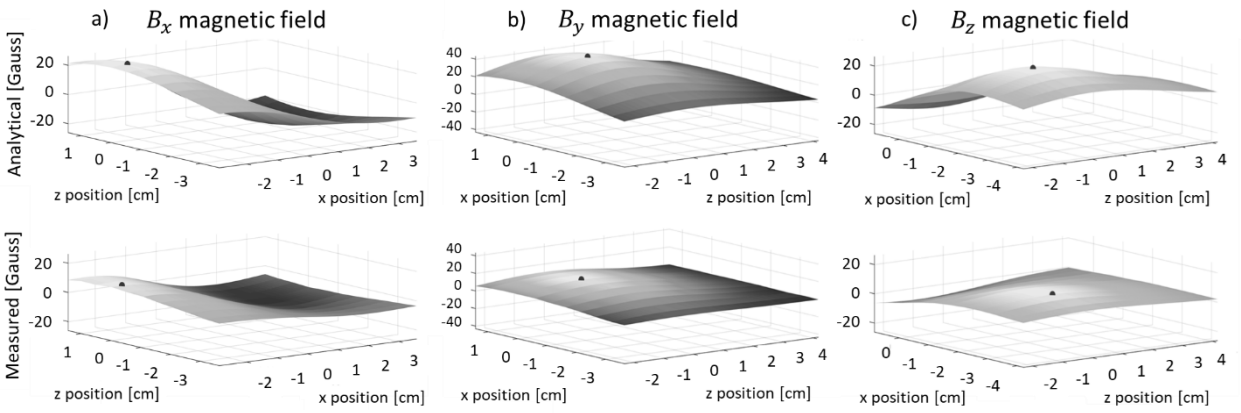

Fig. 3: Topography of magnetic field components with marked extrema points of a centered field-cooled image

IV. Results

A. Frozen Image Model Extrema Verification

For a magnet directly above the center of the field-cooled superconductor, a comparison of frozen image's magnetic field in the three spatial components is shown in Fig. 3. The measured (bottom plot) extrema locations for each magnetic field component are close in proximity to the frozen image model (top plot) extrema locations. Fig. 3.a shows the x-component magnetic field sampled 2.4 cm from the superconductor plane in the y direction.

The analytical prediction and measured (x, z) location exist at (-2.4, 0) cm and (-2.6, 0) cm, a difference of 2 mm between model and measurement. For Fig. 3.b sampled at 3 cm in the y direction, analytical prediction and measured extremum (x, z) location of the y component in magnetic field exist at (0, 0) cm and (-0.2, 0) cm, a difference of 2 mm between model and measurement. For Fig. 3.c sampled at 2.4 cm in the y direction, analytical prediction and measured extremum (x, z) location of the z component in magnetic field exist at (0, -2.2) cm and (0.2, -2.7) cm, a difference of 5 mm between model and measurement. Despite the similarity in extrema location, the measured magnetic field does not match the magnitude of magnetic field predicted by the frozen image model.

B. Frozen Image Model Magnitude Verification

The frozen image model predicts magnetic field gradient or shape accurately for a magnet flux-pinned directly above the center of superconductor but severely overestimates the magnitude of strength of the image. Kordyuk's model does not capture the reduction in image strength as a magnet is imprinted farther away from the reference point. The magnet above the center of field-cooled superconductor is the maximum magnetic flux

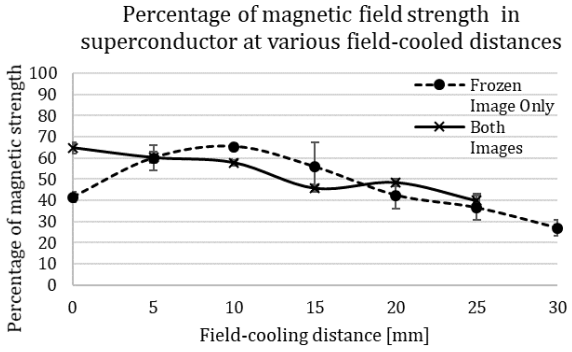

Fig. 4: Average percentage of magnetic field captured within superconductor for a frozen image only and both images scenario. Error bars indicate variation in magnetic field components

observable, yet measurements for the surface normal component of magnetic field is 39% less than the frozen image model prediction, seen at the vertical origin in Fig. 4. The percentage reduction of image magnetic field strength is consistent across all components of magnetic field within an average 4% standard deviation. The sole frozen image and combined images decrease in magnetic field penetration at the same rate[2], depicted in Fig. 4. To implement this magnetic field strength reduction in a dynamic model, the image strength may be scaled by interpolating empirical values in a look-up table or with an approximation.

C. Frozen Image Model Shape Verification

Implied in theory, the frozen image model generates a symmetric potential well because an infinite plane superconductor captures equivalent magnetic flux in all directions. A physical superconductor of finite dimension also generates a symmetric potential well when the field-cooled image is centered. The difference lies in field-cooling the magnet away from the center of the superconductor, producing an asymmetrical imprint of magnetic field due to uneven flux distribution throughout the superconductor volume. The displacement between the predicted extrema location and measured extrema increase as the field-cooling location displaces farther from the center of the superconductor, shown by Fig. 5. Each marker symbol in the legend represents each experiment varying field-cooling distance from center of superconductor.

The potential well extrema locations are displaced from their expected locations, which is emphasized the farther the magnet is cooled from the center of the superconductor. The potential well extrema bias closer to the center of the superconductor, thus the magnetic field over the edge of the superconductor is only partially captured, shown in the comparison of magnetic field

[2] The frozen image experiment at 0 mm field-cooled distance is an outlier. A possible explanation is poor temperature control during the field-cooling process.

level planes of Fig. 6. The level planes help visualize the shape of the potential energy well formed by the magnetic field, specifically in the z component for Fig. 6. This clipping effect contributes not only to the extrema location displacement, but also to the reduction in the magnitude of magnetic field captured in the superconductor.

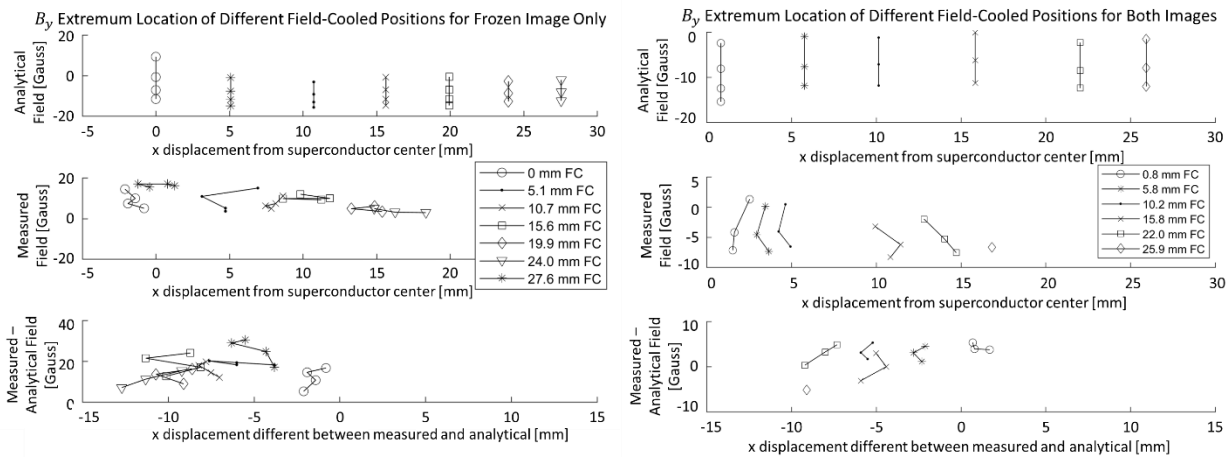

Fig. 5: Left, comparison of frozen image extrema locations from frozen image model (top), measurements (middle), and the difference (bottom) in extrema locations; right, comparison of both images.

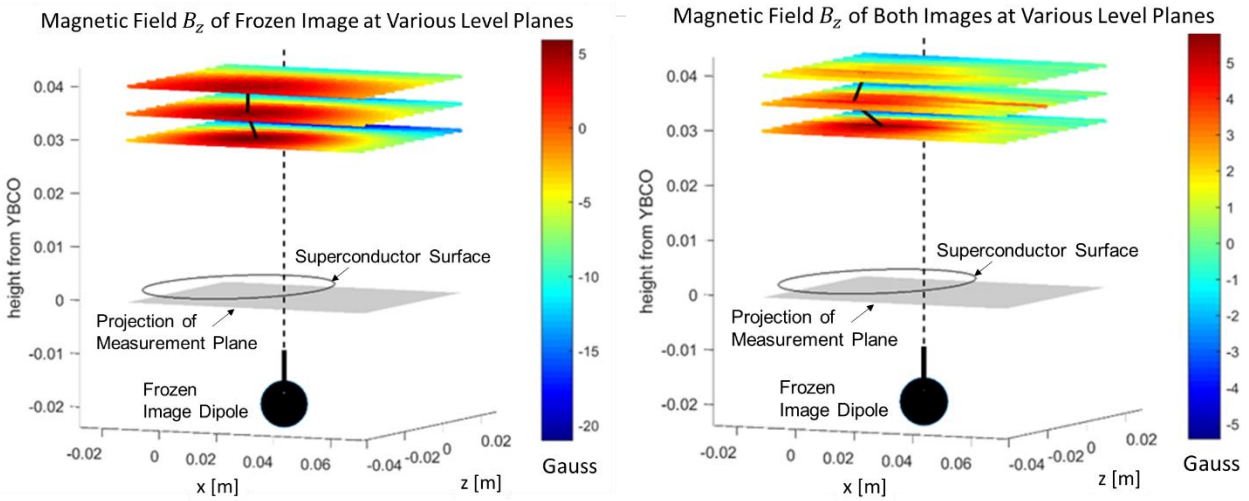

Fig. 6: Magnetic field heat map of z component of magnetic field, for a magnet completely off the field-cooled superconductor surface area (30 mm FC distance over a 28 mm radius superconductor), showing clipped field

D. Finite Dimension Modification in Frozen Image Model

A scalar reduction in magnitude of magnetic field (c_F), given by Eq. (4), describes the reduction in magnetic field strength from finite dimension effect by incorporating the position of the physical magnet ($\boldsymbol{r}$) and superconductor surface normal ($\boldsymbol{a_s}$). Lateral distance from the center of the superconductor (r_l) directly produces this reduction relationship in magnitude of magnetic field. The lateral distance is the projection of the location of the physical magnet onto the superconductor surface from the center of the superconductor ($\boldsymbol{O_s}$), given by Eq. (5) and shown in Fig. 7.

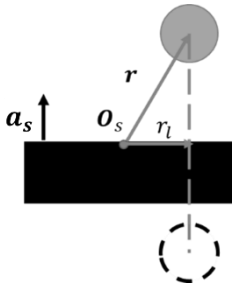

Fig. 7: Parameter definition relevant for finite dimension modification

The reduction scalar (c_F) may be interpolated from a look-up table of measured values or approximated, given by Eq. (6). c_{Fmax} is the percentage of magnetic field captured with the magnet located directly above the center of the superconductor and b_F is the rate of reduction, (c_F), as the magnet displaces farther from the center of the superconductor. The reduction scalar is bounded from 0 to c_{Fmax}. The physical configuration for these experiments yield numerical values $c_{Fmax} = 0.64$ and $b_F = 0.001$ but for different geometries of magnet and superconductor, these parameters may change. The authors suggest quantifying reduction for configurations specific to different systems.

$$c_F = f(\boldsymbol{r}, \boldsymbol{a_s}) \quad (4)$$

$$r_l = |\boldsymbol{r} - (\boldsymbol{r} \cdot \boldsymbol{a_s})\boldsymbol{a_s}| \quad (5)$$

$$c_F = \max(c_{Fmax} - b_F * r_l,\ 0) \quad (6)$$

The general dynamics model includes the reduction scalar by modifying the expressions for the images' magnetic moment dipoles, originally given by Eq. (1) and (2). Eq. (7) and (8) give the modified expressions in which the reduction scalars incorporate the relevant position vectors. The frozen image magnetic moment dipole scales with field-cooled position ($\boldsymbol{r_{FC}}$) and the mobile image with instantaneous magnet position ($\boldsymbol{r}$). The subsequent force and torque equations between the image and physical magnet do not change and are solved with the refined magnetic moment dipole expressions.

$$\boldsymbol{m_f} = c_F(\boldsymbol{r_{FC}}, \boldsymbol{a_s}) * (2(\boldsymbol{a_s} \cdot \boldsymbol{m_{FC}})\boldsymbol{a_s} - \boldsymbol{m_{FC}}) \quad (7)$$

$$\boldsymbol{m_m} = c_F(\boldsymbol{r}, \boldsymbol{a_s}) * (\boldsymbol{m_{mag}} - 2(\boldsymbol{a_s} \cdot \boldsymbol{m_{FC}})\boldsymbol{a_s}) \quad (8)$$

V. Conclusion

From these experiments, a finite dimension effect is clearly visible. Field-cooling a superconductor with the magnet farther away embeds less magnetic flux within the superconductor and modifies the shape of the magnetic field gradient over the edge of the superconductor. A reduction scalar is defined to modify the magnetic moment dipoles of the weaker images. The reduction scalar implies a threshold distance of the magnet from the superconductor to generate a magnetic image. Although this work shows that the finite dimension effect clearly, the proposed finite dimension effect expression is only a preliminary formulation. The expression may be better refined with more measurements of the same experiment or extending to more general geometries of magnets and superconductors. The frozen image model may be used as a basis to simulate dynamics for any arbitrary configuration of magnets and superconductors, with a more accurate model including finite dimension effects.

Acknowledgment

This research was in part funded through NSTRF under proposal NNX15AP55H.

This research was carried out at the Jet Propulsion Laboratory, California Institute of Technology, under a contract with the National Aeronautics and Space Administration and funded through the internal Research and Technology Development program.

References

[1] C. Navau, N. Del-Valle, and A. Sanchez, "Macroscopic Modeling of Magnetization and Levitation of Hard Type-II Superconductors: The Critical-State Model," *IEEE Trans. Appl. Supercond.*, vol. 23, no. 1, p. 8201023, 2013.

[2] A. Sanchez and C. Navau, "Critical-current density from magnetization loops of finite high- T c superconductors," *Supercond. Sci. Technol.*, vol. 14, no. 7, p. 444, 2001.

[3] A. A. Kordyuk, "Magnetic levitation for hard superconductors," *J. Appl. Phys.*, vol. 83, no. 1, pp. 610–612, Jan. 1998.

[4] F. Zhu and M. Peck, "Linearized Dynamics of General Flux-Pinned Interfaces," *IEEE Trans. Appl. Supercond.*, vol. 28, no. 8, pp. 1–10, Dec. 2018.

[5] F. Zhu, L. Jones-Wilson, and M. Peck, "Flux-Pinned Dynamics Model Parameterization and

Sensitivity Study," presented at the IEEE Aerospace Conference, Big Sky, Montana, 2018.

[6] M. K. Alqadi, F. Y. Alzoubi, H. M. Al-khateeb, and N. Y. Ayoub, "Interaction between a point magnetic dipole and a high-temperature superconducting sphere," *Phys. B Condens. Matter*, vol. 404, no. 12, pp. 1781–1784, Jun. 2009.

[7] Z. Ren *et al.*, "Influence of shape and thickness on the levitation force of YBaCuO bulk HTS over a NdFeB guideway," *Phys. C Supercond.*, vol. 384, no. 1, pp. 159–162, Jan. 2003.

[8] H. Teshima, M. Sawamura, M. Morita, and M. Tsuchimoto, "Levitation forces of a single-grained Y-Ba-Cu-O bulk superconductor of 48 mm in diameter," *Cryogenics*, vol. 37, no. 9, pp. 505–509, 1997.

[9] W. M. Yang *et al.*, "The effect of magnet configurations on the levitation force of melt processed YBCO bulk superconductors," *Phys. C Supercond.*, vol. 354, no. 1, pp. 5–12, May 2001.

[10] B. F. Edwards, D. M. Riffe, J.-Y. Ji, and W. A. Booth, "Interactions between uniformly magnetized spheres," *Am. J. Phys.*, vol. 85, no. 2, pp. 130–134, Jan. 2017.